POLITECNICO DI TORINO
Repository ISTITUZIONALE

VHCF Response of H13 Steels Produced with Different Manufacturing Processes

Availability:
This version is available at: 11583/2656821 since: 2017-05-25T13:03:39Z

(Article begins on next page)

28 April 2024

XVIII International Colloquium on Mechanical Fatigue of Metals (ICMFM XVIII)

VHCF response of H13 steels produced with different manufacturing processes

A. Tridello[a]*, D.S. Paolino[b], G. Chiandussi[c], M. Rossetto[d]

[a,b,c,d]Department of Mechanical and Aerospace Engineering, Politecnico di Torino, Turin, Italy

Abstract

Experimental results have recently shown that failures at stress amplitude below the conventional fatigue limit and at Very High Cycle Fatigue (VHCF) are possible. In case of high-strength steels, VHCF failures generally originate from defects/inclusions present within the material and, consequently, the defect population properties (size and quantity) significantly affect the VHCF response of high-strength steels.

Different refinement processes are commonly adopted in order to improve steel cleanliness: among the other, the ElectroSlag Remelting (ESR) process allows to obtain very clean high-strength steels, thus possibly inducing a significant enhancement of the VHCF response.

The present paper aims at investigating the actual effect of the ESR process on the VHCF behavior of an AISI H13 steel. Fully reversed ultrasonic tension-compression tests are carried out on hourglass specimens manufactured with and without the ESR process. The estimated P-S-N curves highlight the positive effects of the ESR process on the VHCF response of the investigated H13 steel.

Keywords: Very High Cycle Fatigue (VHCF); Electroslag remelting (ESR); inclusion content; ultrasonic testing; hydrogen embrittlement.

1. Introduction

In recent years, the Very-High-Cycle Fatigue (VHCF) response of metallic materials has become a major point of interest for researchers and industries. A particular attention in the VHCF literature is devoted to high-strength steels, for their wide usage in critical structural components subject to failures at very high number of cycles. As

* Corresponding author. Tel.: +39 011 090 6913.
  E-mail address: andrea.tridello@polito.it

reported in the literature, high-strength steels generally exhibit unexpected VHCF failures (at stress amplitude below the conventional fatigue limit [1]) with cracks nucleating from defects and inclusions originated during the manufacturing process. The defect population and, in particular, the characteristic defect size therefore significantly affect the VHCF response of high-strength steels [2].

Defects and inclusions in high-strength steels generally form during the production process (in particular during the melting and the pouring processes). In order to enhance the cleanliness of high-strength steels, different refinement processes are commonly adopted in manufacturing industries. Among them, it is generally acknowledged that the ElectroSlag Remelting (ESR) process yields the removal of large inclusions and defects, thus possibly inducing a strong enhancement of the VHCF response.

The present paper aims at assessing the actual influence of the ESR process on the VHCF response of an AISI H13 steel. Experimental tests are run on specimens produced with and without the ESR process. Fully reversed tension-compression tests are carried out on hourglass specimens by using the ultrasonic testing machines developed at the Politecnico di Torino. Fracture surfaces are observed by using the Scanning Electron Microscope (SEM) in order to investigate the origin of VHCF cracks and to compare the type of defects originating failure before and after the ESR process [3]. Experimental results are analyzed and compared according to a statistical model recently developed by the authors [4] and based on the hydrogen assistance crack growth theory proposed by Murakami [2].

Nomenclature

ESR	ElectroSlag Remelting process
H13	AISI H13 steel obtained by conventional casting
H13 ESR	AISI H13 steel obtained by conventional casting and subjected to ESR process
$\sqrt{a_{d,0}}$	square root of the projected area of the inclusion originating failure
$F_{\sqrt{A_{d,0}}}$	type 1 LEV (Largest Extreme Value) cumulative distribution function
σ_l	fatigue limit

---

2. Experimental material

AISI H13 steel (EN 40CrMOV5-1 steel according to UNI EN ISO 4957) is a hot work tool steel, but it is also used for components subjected to failures at very high number of cycles (i.e., fuel injectors for naval engines and aerospace components). The chemical compositions of the investigated AISI H13 steel is reported in Table 1:

Table 1. Chemical composition of the AISI H13 steel

Element	C	Si	Mn	Cr	Mo	V
Mass (%)	0.39	1.0	0.4	5.3	1.3	0.9

Two different types of H13 steels are used for the experimental tests: Orvar 2M and Supreme ESR by Uddeholm. The Orvar 2M H13 steel (commercial name Orvar 2M) is obtained by conventional casting. The Supreme ESR H13 steel (commercial name H13 Supreme) is twice melted with an Electro Slag Remelting process, which permits the removal of large defects and inclusions from the original steel, thus significantly enhancing the steel cleanliness.

Hourglass specimens are used for the experimental tests: the specimen shape is obtained through a CNC process starting from rectangular bars with dimensions 32x32x115 mm. The specimen is designed analytically and verified through Finite Element Analysis (FEA). The specimen risk-volume (volume of material subjected to a stress amplitude above the 90% of the maximum stress [5,6]) is equal to 194 mm^3. The stress concentration factor is verified to be below 1.07 through FEA. The specimen geometry is shown in Fig. 1.
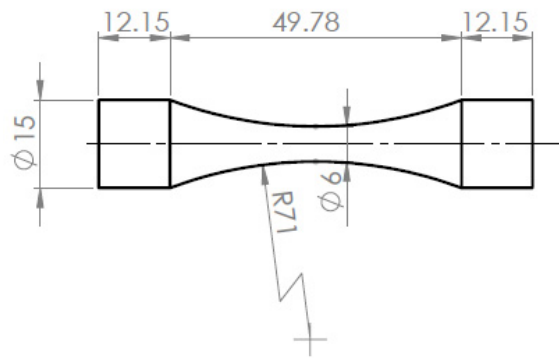
Fig. 1. Hourglass specimen geometry used for the experimental tests.

After the machining process the specimen is quenched and tempered in an ordinary industrial cycle in order to obtain a homogeneous tempered martensite microstructure. The heat treatment involves: preheating at 1023 K, austenitizing at 1030 K, gas quenching and three tempering cycles: first tempering at 793 K, second and third tempering at 813 K.

The mechanical properties of the two investigated H13 steels are experimentally evaluated. The Young modulus (211.8 GPa for the H13 steel and 212.9 GPa for the H13 ESR steel) and the ultimate strength (2000 MPa for the H13 steel and 2100 MPa for the H13 ESR steel) are slightly larger for the H13 ESR steel. The Vickers hardness, evaluated according to [7], is equal for the two steels ($HV = 560$). Due to the limited difference, the mechanical properties of the two investigated H13 steels can be considered the same.

In order to enhance the nucleation of cracks due to internal defects and to avoid unexpected failures from superficial defects, specimens are fine polished before each experimental test with sand papers with increasing grit (from 200 to 1200).

3. Experimental setup

Fully reversed tension-compression tests are carried out by using the ultrasonic testing machines developed at the Politecnico di Torino [3]. Fatigue tests are carried out up to failure or up to 10^{10} cycles (runout). A closed-loop control based on the displacement measured at the specimen free end ensures a constant stress amplitude in the specimen mid-section. The displacement amplitude is measured in real-time during the test with a laser displacement sensor (sample rate of 300 kHz). An accurate strain gage calibration is performed before each experimental test in order to correlate the stress amplitude in the specimen mid-section and the displacement amplitude at the specimen free end.

Specimen temperature is continuously monitored during the experimental tests by using an infrared sensor in order to limit the specimen self-heating due to internal dissipation [8]. The test is automatically stopped when the specimen temperature exceeds the upper allowable temperature (303 K) and restarted when the temperature falls below 298 K (intermittent tests [9]). Vortex tubes are also employed to limit the temperature increment and to speed up the specimen cooling. The temperature variation in the radial direction is verified through FEA and is smaller than 1%. The temperature in the specimen risk-volume is therefore considered uniform during the test. The actual frequency of the test (frequency evaluated by taking into account the pause phase in the intermittent test) is maintained above 15 kHz for each test.

Fig. 2 shows the measuring system (laser displacement sensor and infrared temperature sensor) and the vortex tubes in a typical configuration during an ultrasonic test.

Fig. 2. Typical measuring system configuration in an ultrasonic test.

4. Experimental results

Table 2 summarizes the experimental tests carried out for the two types of H13 steel: the stress amplitude in the specimen center (nominal stress amplitude) is reported.

Table 2. Experimental results.

	Number of specimens	Minimum stress [MPa]	Maximum stress [MPa]	Number of runouts
H13	15	570	710	3
H13 ESR	16	630	810	3

In order to determine the crack origin, fracture surfaces are observed through Scanning Electron Microscope (SEM): all the fractures originated from inclusions present within the material (Section 5.1). Fig. 3 shows the distribution of inclusions originating failure within the risk-volume. The abscissa axis reports the location of the inclusions originating failure in the longitudinal direction z (normalized with respect to the maximum distance from the specimen center of a fatigue failure, $L_{max,f}$). The ordinate axis shows the position of the inclusions in the radial direction r_f (normalized with respect to the specimen radius at the corresponding longitudinal position, r).
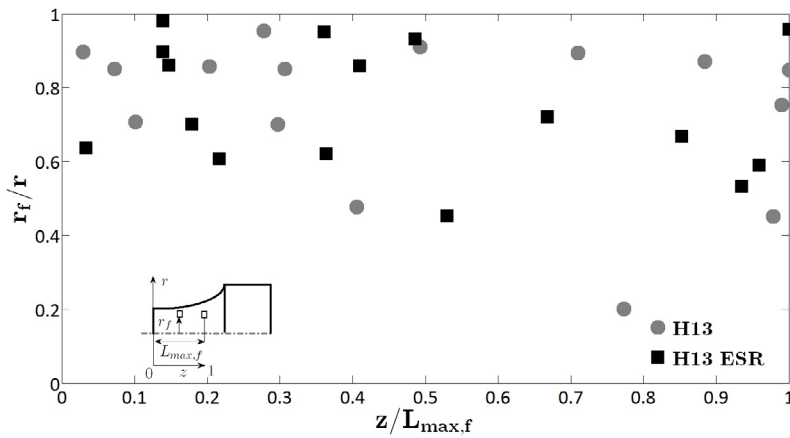

Fig. 3. Distribution of failures within the risk-volume.

According to Fig. 3, failures are uniformly distributed within the risk-volume both for the H13 steel and for the H13 ESR steel, thus confirming the homogeneity of the microstructure after the heat treatment. In order to take into account the stress variation within the risk-volume and to assess the actual stress amplitude causing crack nucleation, the stress amplitude in the vicinity of the initial defect is evaluated through FEA (actual stress). The actual stress is considered as the applied stress during each experimental test, in the following.

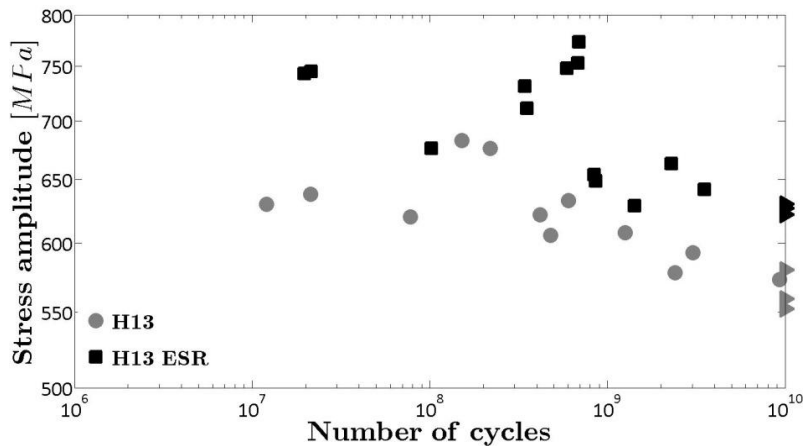Fig. 4 shows the S-N plot of the experimental data.

Fig. 4. S-N plot of the experimental data.

5. Inclusion analysis and P-S-N curves

Fracture surfaces are observed through an optical microscope and through a SEM. The chemical composition, the morphology of the inclusions originating failure and the statistical distribution of the inclusion size in the two H13 steels are compared in Section 5.1.

All fracture surfaces show a fish-eye morphology [2], with an Optically Dark Area (ODA) in the vicinity of the initial inclusion. According to [2], the crack growth inside the ODA occurs with the assistance of the hydrogen accumulated near the initial inclusion. In order to take into account the contribution of the hydrogen in the crack growth, the experimental data are analyzed by considering a model recently proposed in [4] and based on the hydrogen assistance crack growth theory proposed by Murakami [2]. In particular, the hydrogen contribution is modelled in [4] by considering an additional stress intensity factor which contributes to crack growth in combination with the stress intensity factor associated to the inclusion dimension. Following the procedure reported in [4], the P-S-N curves for the two investigated steels are estimated and compared in Section 5.2.

5.1. SEM analysis

According to the SEM analysis, the same type of inclusions originates fatigue cracks in the two investigated H13 steels. All the inclusions are non-metallic oxide type inclusions with a large percentage of Aluminium, Calcium and Manganese, formed during the steel production process. In particular, 33 out of 34 inclusions show a spherical shape: in one case, a cluster of small inclusions is at the origin of the fatigue failure in the H13 ESR. However, since there is no difference between the chemical composition and the morphology of the inclusions originating failure in the two H13 steels, the critical inclusions before and after the ESR process are the same.

Fig. 5 shows a typical spherical inclusion and the cluster of inclusions found experimentally.
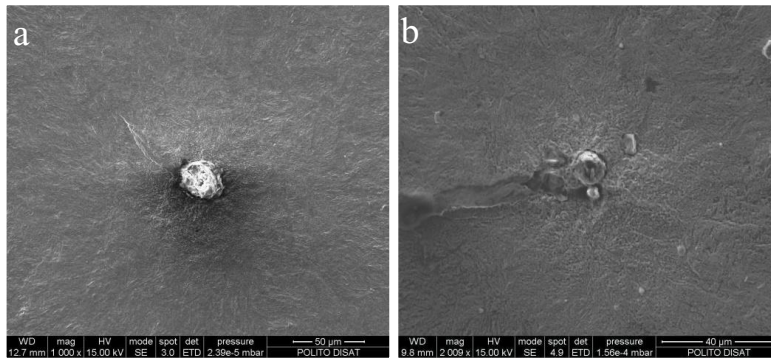
Fig. 5: Different types of inclusions: (a) spherical inclusion; (b) cluster of small inclusions in H13 ESR.

In order to compare the inclusion size in the two H13 steels, the distribution of the inclusion size ($\sqrt{a_{d,0}}$, the square root of the projected area of the inclusion) is estimated. According to [2], the inclusion at the origin of the fatigue crack is the largest inclusion present within the risk-volume; therefore $\sqrt{a_{d,0}}$ follows a Type 1 Largest Extreme Value Distribution (LEVD). Runout specimens are tested at larger stress amplitude up to failure in order to determine the largest inclusion present within the risk-volume. The parameters of the distribution are estimated through the Maximum Likelihood Principle. Fig. 6 shows the Gumbel plot of the inclusions originating failure, together with the estimated distribution $F_{\sqrt{A_{d,0}}}$.
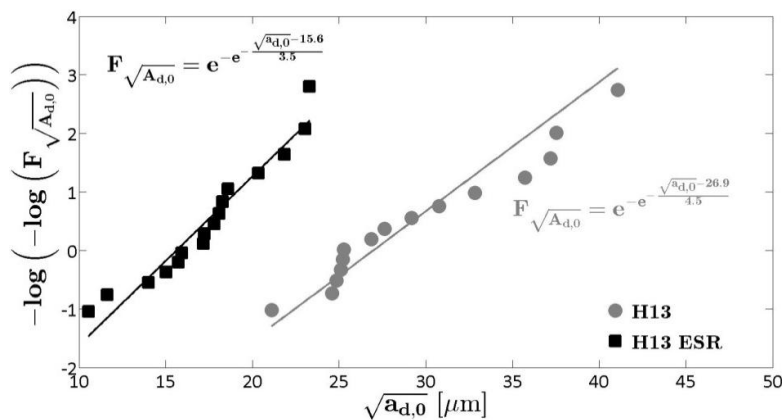

Fig. 6. Gumbel plot of the inclusion size.

According to Fig. 6, inclusions originating failures are larger in the H13 steel. The largest inclusion in the H13 ESR (23.3 μm) is about half of the largest inclusion present within the remelted steel (41.0 μm). Moreover, 14 inclusions out of 15 in the H13 steel are larger than the largest inclusion in the H13 ESR steel.

Therefore, according to the SEM analysis, after the ESR process, larger non-metallic spherical inclusions are removed and the remaining inclusions are significantly smaller than the inclusions in the original H13 steel, with a significant enhancement of the steel cleanliness.

5.2. P-S-N curves

The effect of the different inclusion size on the VHCF response is investigated in this Section by comparing the P-S-N curves. The P-S-N curves for the two H13 steels (Fig. 7) are estimated following the procedure proposed in [4] and by considering the inclusion size distribution determined in Section 5.1.
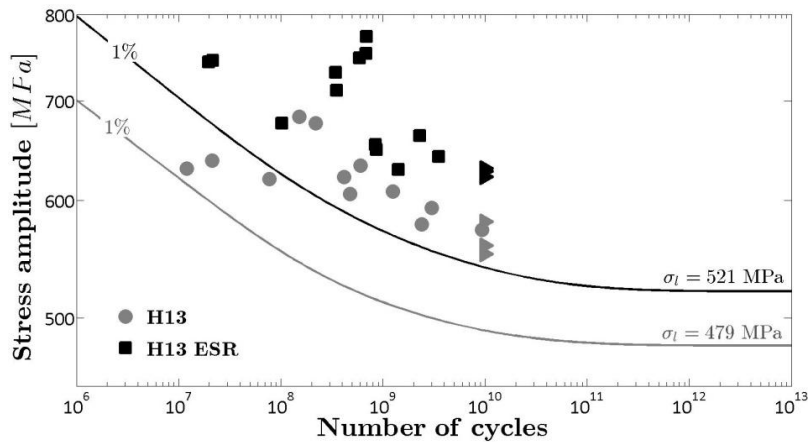

Fig. 7. 1-th P-S-N curves for the two investigated H13 steels.

According to Fig. 7, all failures are above the 1%-th P-S-N curve both for the original and the remelted H13 steels, confirming the validity of the model considered for the analysis of the data. The curve for the H13 ESR steel lays entirely above the curve for the non remelted H13 steel. The difference is significant: if the fatigue limit (σ_l) is taken into account, the difference is larger than 8%. The removal of larger inclusions through the ESR process strongly influences the VHCF response of the investigated H13 steels. Indeed, since the initial inclusions are the same before and after the ESR process (i.e., oxide type spherical inclusions, according to Section 5.1), the different inclusion size is the main reason for the different VHCF behavior. Moreover, it can be noted that larger inclusions are generally characterized by larger trapping sites which allow for larger accumulation of hydrogen. Therefore, it is possible that the small inclusions in the H13 ESR are characterized by smaller hydrogen concentration, thus further contributing to the enhancement of the VHCF response after the ESR process.

To conclude, the experimental results confirm the positive effect of the ESR process on the VHCF response of the H13 steel. Therefore, the ESR refinement process can be employed when high performance and high VHCF resistance are needed.

6. Conclusions

The effect of the ElectroSlag Remelting process (ESR) on the VHCF response of an AISI H13 steel was investigated in the paper. Ultrasonic VHCF tests were carried out on an AISI H13 steel obtained by conventional casting and on an AISI H13 subjected to the ESR process. Fracture surfaces were observed by using the Scanning Electron Microscope in order to analyze the origin of the fatigue crack. All the failures originated from an internal inclusion within the material: no difference was found in the inclusion type before and after the ESR process. In particular, spherical oxide type inclusion were at the origin of the fatigue crack in 24 out of 25 failures (one failure was due to a cluster of small inclusions). However, inclusions originating failures in the remelted steel were significantly smaller: the largest inclusions in the original H13 steel was found to be two times the largest inclusion found in the H13 ESR steel. The experimental results highlighted a significant removal of larger inclusions through the ESR process.

Finally, the experimental results are analyzed and compared according to a statistical model recently proposed.

The estimated P-S-N curves highlighted the significant enhancement of the VHCF response attainable through the ESR process. In particular, if the fatigue limit is taken into account, the difference is larger than 8%. The removal of large inclusions through the ESR was found to be the main reason for the enhancement of the VHCF behavior of the H13 steel after the ESR process. The ESR refining process therefore can be employed when high resistance in the VHCF regime is required.

Acknowledgements

References

[1] C. Bathias, There is no infinite fatigue life in metallic materials, Fatigue Fract. Eng. Mater. Struct. 22 (1999), 559-565.
[2] Y. Murakami, Metal Fatigue: Effects Of Small Defects And Nonmetallic Inclusions. Elsevier, Oxford, 2002.
[3] D.S.Paolino, M. Rossetto, G. Chiandussi, A. Tridello, Sviluppo di una macchina a ultrasuoni per prove di fatica gigaciclica, 41th AIAS Conference, Vicenza (2002), In Italian.
[4] D.S. Paolino, A. Tridello, G. Chiandussi, M. Rossetto, S-N curves in the very-high-cycle fatigue regime: statistical modeling based on the hydrogen embrittlement consideration, Fatigue Fract. Eng. Mater. Struct. (In press), DOI: 10.1111/ffe.12431.
[5] Y. Furuya, Notable size effects on very high cycle fatigue properties of high strength steel. Mater. Sci. Eng. A 528 (2011) 5234–5240.
[6] D.S. Paolino, A. Tridello, G. Chiandussi, M. Rossetto, On specimen design for size effect evaluation in ultrasonic gigacycle fatigue testing. Fatigue Fract. Eng. Mater. Struct. 37 (2014) 570-579.
[7] EN ISO 6507-1 (2005) Metallic materials - Vickers hardness test - Part 1: Test method, International Standard Organization, Genève, (2005).
[8] A. Tridello, D.S. Paolino, G. Chiandussi, M. Rossetto, Gaussian specimens for VHCF tests: Analytical prediction of damping effects, Int. J. Fatigue 83 (2016) 36-41.
[9] S. Stanzl-Tschegg, Very high cycle fatigue measuring techniques. Int. J. Fatigue 60 (2014) 2-17.